Method of generating orthoscopic elemental image array from sparse camera array

Huan Deng (邓 欢)[1], Qionghua Wang (王琼华)[1,2*], and Dahai Li (李大海)[1]

[1]*School of Electronics and Information Engineering, Sichuan University, Chengdu 610065, China*

[2]*State Key Laboratory of Fundamental Science on Synthetic Vision, Sichuan University, Chengdu 610065, China*

[*]*Corresponding author: qhwang@scu.edu.cn*

Received December 29, 2011; accepted March 14, 2012; posted online May 11, 2012

We propose a method of generating orthoscopic elemental image array from a sparse camera array. A parallax image array obtained by a sparse camera array provides different perspectives of a real three-dimensional (3D) scene, and has all the information the elemental image array needs. In-depth analysis of the generation method and the relationships between the sparse camera array and the elemental image array are presented. The experimental results demonstrate the correctness of the proposed method.

OCIS codes: 110.3010, 110.6880, 120.2040.

doi: 10.3788/COL201210.061102.

In 1908, Lippmann first proposed the three-dimensional (3D) display based on integral imaging (II)[1]. It is considered as one of the most attractive 3D displays, because it presents true 3D images with full parallax and full color information in continuous viewing points, without using special glasses and coherent light[2−4]. One problem encountered with II, however, is the pseudoscopic nature. Okano proposed to rotate each elemental image by 180° around the center of the elemental image[5], however, the method only provides virtual 3D scene, which is behind the display screen. When the two-step pickup method is proposed[6], a smart pixel mapping algorithm is deduced to realize the secondary pickup process in a computer[7−8]. However, the smart pixel mapping algorithm is limited since it only allows a fixed position for the reconstructed scene and the number of micro-lenses. Another algorithm, called smart pseudoscopic-to-orthoscopic conversion (SPOC), has been proposed, which allows the conversion from pseudoscopic to orthoscopic with full control over the display parameters, so that one can generate an elemental image array that suits the characteristics of the II display system[9]. However, it is not arbitrary in selecting the parameters of the SPOC algorithm, resulting in the lack of information or redundant information.

One can see different perspectives of a reconstructed 3D scene at different viewing points when seeing an II display system. On the contrary, based on the principle stating that rays are retrievable, we generate an elemental image array (EIA) from different perspectives of a real 3D scene called parallax image array (PIA) in this letter. Here, we propose a generation method of orthoscopic EIA from a sparse camera array, which updates the SPOC algorithm. Based on the theory of the II reconstruction, in-depth analysis of the generation method and the process of selecting the parameters are presented.

An II display system, including an EIA and a micro-lens array, can reconstruct a 3D scene which is the same as the original 3D scene. At a viewing point, one can see a pixel through each micro-lens; moreover, pixels obtained from all the elemental images form a parallax image of the reconstructed 3D scene with the resolution being equal to the number of elemental images. At different viewing points, one can obtain a PIA of the reconstructed 3D scene, just like shooting a real 3D scene using a sparse camera array. On the contrary, based on the principle stating that rays are retrievable, we can generate an EIA from a PIA using a sparse camera array.

Our proposed generation method of orthoscopic EIA has two processes: capturing the PIA and generating the EIA (Fig. 1).

In capturing the PIA, it is necessary to know the parameters of the II display system. The pitch, the number, and the resolution of the required elemental images are p, $M \times N$, and r, respectively, and the focal length of the micro-lens in the II display system is f. The sparse camera array includes $M' \times N'$ cameras, and the optical axis of each camera is parallel to each other, with the uniform spacing d and the focal length f', as shown in Fig. 1(a). A PIA including $M' \times N'$ parallax images is obtained using the sparse camera array.

In generating the EIA, as shown in Fig. 1(b), a pinhole array with the function of the sparse camera array is used to reconstruct a virtual 3D scene. The pitch and the number of the pinhole array are d and $M' \times N'$, respectively, and the gap between the pinhole array and the PIA is f'. Each parallax image is rotated by 180° around its center, and a virtual 3D scene is reconstructed, which is just the same as the original 3D scene. Then, a micro-lens array is used to capture the reconstructed virtual 3D scene.

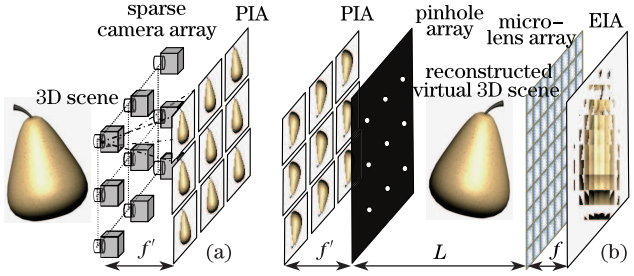

Fig. 1. Schematic of the proposed generation method of orthoscopic EIA. (a) Capture of the PIA and (b) generation of the EIA.

The distance between the pinhole array and the micro-lens array L determines the position of the reconstructed 3D scene. Each micro-lens has its own perspective in the reconstructed virtual 3D scene, and the EIA is obtained on the focal plane of the micro-lens array.

To ensure that the sparse camera array captures neither more nor less information than the required EIA, we select the parameters of the sparse camera array carefully. For a single elemental image, r cameras are needed to capture the r pixels at r different positions since the resolution of an elemental image is r (Fig. 2). Therefore, the distance between adjacent cameras in the sparse camera array d can be deduced as

$$d = \frac{pL}{rf}. \tag{1}$$

For the II display system, which has $M \times N$ elemental images, the sparse camera array should cover the whole viewing zone at the viewing distance L in order to obtain sufficient information. Therefore, based on the geometric relationships in Fig. 2, the number of cameras in the sparse camera array $M' \times N'$ can be deduced as

$$\begin{cases} M' = \text{ceil}\left(\dfrac{rfM + Lr}{L}\right) \\ N' = \text{ceil}\left(\dfrac{rfN + Lr}{L}\right) \end{cases}, \tag{2}$$

where function ceil$(\cdot)$ rounds a number to the largest integer. We obtain $M' \times N'$ parallax images from the sparse camera array with the resolution $M \times N$, which is equal to the number of the elemental images in the EIA.

The generation of the EIA is performed using a pixel mapping algorithm in a computer. Figure 3 shows the mapping relationships from the PIA to the EIA. In the m'th column and the n'th row parallax image, a pixel in the i'th column and the j'th row is denoted as $I'(m', n')_{i',j'}$. The rays emitted from the pixel $I'(m', n')_{i',j'}$ are transmitted by the m'th column and the n'th row pinhole, and then refracted by the mth column and the nth row micro-lens in the micro-lens array. Finally, the rays arrive at the ith column and the jth row pixel of the mth column and the nth row elemental image in the EIA, and the pixel is denoted as $I(m, n)_{i,j}$.

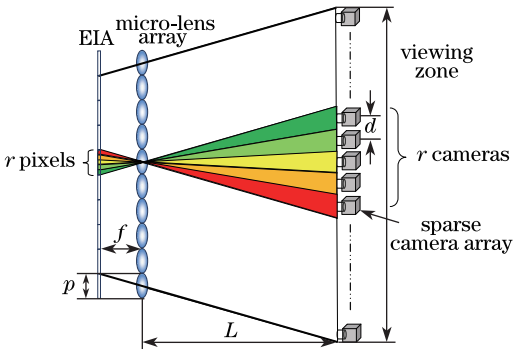

Fig. 2. Schematic of the selection of parameters in the sparse camera array.

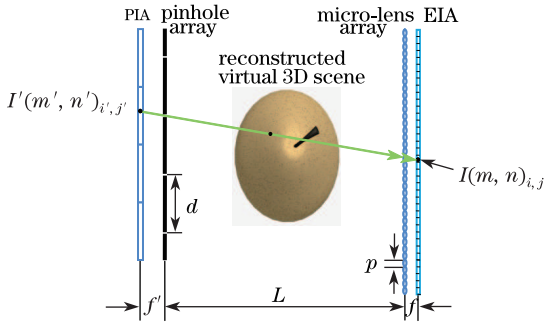

Fig. 3. Mapping relationships between the PIA and the EIA.

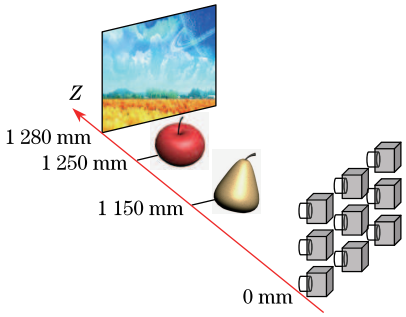

Fig. 4. 3D scene.

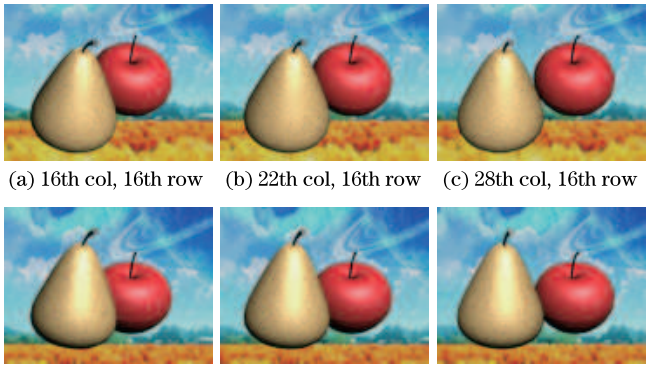

(a) 16th col, 16th row (b) 22th col, 16th row (c) 28th col, 16th row

(d) 16th col, 30th row (e) 22th col, 30th row (f) 28th col, 30th row

Fig. 5. Six parallax images of the PIA obtained using the sparse camera array.

Therefore, the pixel $I'(m', n')_{i',j'}$ in the PIA corresponds to the pixel $I(m, n)_{i,j}$ in the EIA. Thus, we can obtain Eq. (3) as

$$I(m, n)_{i,j} = I'(m', n')_{i',j'}. \tag{3}$$

The values of m, n, i and j in Eq. (3) can be obtained using

$$\begin{cases} m = i' \\ n = j' \end{cases}, \tag{4}$$

$$\begin{cases} i = \text{round}\left[r/2 + fr\dfrac{(M'/2 - m' + 1)d + (M/2 - i' - 1)p}{pL}\right] \\ j = \text{round}\left[r/2 + fr\dfrac{(N'/2 - n' + 1)d + (N/2 - j' - 1)p}{pL}\right] \end{cases}, \tag{5}$$

where function round $(\cdot)$ rounds a number to the nearest integer. When the calculated i or j is bigger than r, the pixel should be abandoned in order to eliminate the overlapping between adjacent elemental images. In this way, in loop m' from 1 to M', n' from 1 to N', i' from 1 to M, and j' from 1 to N, all the pixels in the PIA are mapped to the focal plane of the micro-lenses, thus

forming an EIA. The pitches of the elemental image and the micro-lens are both p, and the number of elemental images in the EIA is denoted by $M \times N$.

The position of the reconstructed 3D scene can be adjusted by changing the distance between the pinhole array and the micro-lens array L. We assume that the distance between the 3D object and the sparse camera array is l. When l=L, the 3D object is displayed on a screen; if $l > L$ or $l < L$, the 3D object is displayed behind of or in front of a screen.

In our experiment, a 3D scene and a sparse camera array are built using the 3DS MAX modeling software, and the 3D scene includes a background image, an "apple" and a "pear," as shown in Fig. 4. The Z axis shows the distances between the 3D objects and the sparse camera array, and these are 1 280, 1 250 and 1 150 mm, respectively. The parameters of the experiment are shown in Table. 1. Figure 5 shows six parallax images of the PIA obtained by the sparse camera array. Meanwhile, Fig. 6 shows the EIA generated using the pixel mapping algorithm illustrated above; the total pixel number of the EIA is 6 000×5 400.

The obtained EIA is used for optical reconstruction experiment. The reconstructed 3D scene does not suffer from the pseudoscopic problem. The "pear" appears out of the display screen, and the background image and "apple" appear into the display screen. Figure 7 shows the reconstructed 3D scene in different viewing points, all corresponding to six parallax images are shown in Fig. 5.

To testify the depth of the reconstructed 3D scene, computational reconstruction experiment was carried out, and a series of plane images were digitally obtained at different depths. As shown in Fig. 8, the background image, "apple" and "pear" are clearly obtained at depths of −80, −50 and 50 mm, respectively, as they are originally located. The results indicate that the proposed generation method restores the reconstructed 3D scene with its original size and depth as the conventional II does.

In conclusion, the proposed method generates an orthoscopic EIA from a sparse camera array. The parameters of the sparse camera array are strictly deduced to obtain neither more nor less information than the required EIA.

Table 1. Parameters of the Experiment

M'	d (mm)	f' (mm)	L (mm)	$M \times N$	r	f (mm)	p (mm)
45×44	16.93	50	1 200	200×180	30	3	1.27

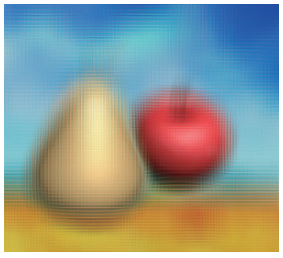

Fig. 6. EIA generated by the proposed generation algorithm.

(a) Upper left view (b) Upper middle view (c) Upper right view

(d) Lower left view (e) Lower middle view (f) Lower right view

Fig. 7. Six perspectives of the reconstructed 3D scene.

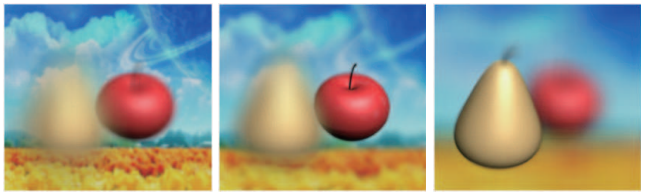

(a) (b) (c)

Fig. 8. Plane images obtained at (a) −80 mm, (b) −50 mm, and (c) 50 mm.

The number of cameras in the sparse camera array is much fewer than the number of elemental images in the EIA, and the process of capturing the PIA is much simpler than that for EIA in the conventional II. The orthoscopic EIA is generated by a computer using the deduced pixel mapping algorithm, and no image degradation occurs. The position of the reconstructed 3D scene can be adjusted by changing the distance between the pinhole array and the sparse camera array. The optical and computational reconstruction experiments demonstrate that the reconstructed 3D scene restores its original size and depth as the conventional II does.

This work was supported by the National Natural Science Foundation of China under Grant No. 61036008.

References

1. G. Lippmann, Comptes-Rendus Acad. Sci. **146,** 446 (1908).
2. J. H. Park, K. Hong, and B. Lee, Appl. Opt. **48,** H77 (2009).
3. J. Hahn, Y. Kim, E. H. Kim, and B. Lee, Opt. Express **16,** 13969 (2008).
4. Q. H. Wang, H. Deng, T. T. Jiao, D. H. Li, and F. N. Wang, Chin. Opt. Lett. **8,** 512 (2010).
5. F. Okano, H. Hoshino, J. Arai, and I. Yuyama, Appl. Opt. **36,** 1598 (1997).
6. H. E. Ives, J. Opt. Soc. Am. A **21,** 171 (1931).
7. D. H. Shin, B. G. Lee, and E. S. Kim, Opt. Lasers Eng. **47,** 1189 (2009).
8. M. Martinez-Corral, B. Javidi, R. Martinez-Cuenca, and G. Saavedra, Opt. Express **13,** 9175 (2005).
9. H. Navarro, R. Martinez-Cuenca, G. Saavedra, M. Martinez-Corral, and B. Javidi, Opt. Express **18,** 25573 (2010).